Laser-induced fragmentation of carbonyl iron as a clean method to enhance magnetorheological effect

Laser-induced fragmentation of carbonyl iron as a clean method to enhance magnetorheological effect

Martin Cvek[a] *, Rafael Torres-Mendieta[b], Ondrej Havelka[b], Michal Urbanek[a], Tomas Plachy[a], Miroslav Cernik[b]

[a]*Centre of Polymer Systems, University Institute, Tomas Bata University in Zlin, Trida T. Bati 5678, 760 01, Zlin, Czech Republic*

[b]*Institute for Nanomaterials, Advanced Technologies and Innovation, Technical University of Liberec, Studentska 1402/2, 461 17, Liberec, Czech Republic*

**Corresponding author. E-mail address: cvek@utb.cz (M. Cvek).*

ABSTRACT

Magnetic nanoparticles (NPs) are widely used as additives in magnetorheological (MR) suspensions to enhance their magnetic performance and kinetic stability. The synthesis of NPs is often resolved via chemical routes or complex manufacturing procedures, which require hazardous chemicals and generate waste products. In this study, a clean, laser-mediated strategy known as laser fragmentation in liquids (LFL) is proposed that enables the synthesis of NP-based additives directly from the given MR suspension, with the added advantage of limiting the production of waste during the fabrication process. The carbonyl iron (CI) microparticles dispersed in ethylene glycol were used as both the MR suspension and precursor agent in the production of the nanoscale additive. The size and crystalline structure of the NPs were investigated via TEM and XRD, respectively. The mixture of the MR suspension and laser-synthesized additive notably facilitated the magnetisation of the CI particles, incrementing the MR characteristics and dynamic yield stress values by up to 31% in a low-to-moderate field region, which are important aspects in various field-controlled robotic, damping and torque systems. The concept presented appears to be an effective and clean alternative for fabricating bidispersed MR suspensions through the nanoscale additive approach.

Keywords: Magnetorheology, nanoparticle fabrication, laser fragmentation in liquids, magnetism, suspension, additive

1. Introduction

Mixtures of magnetically-permeable microparticles in nonmagnetic liquids are known as magnetorheological (MR) suspensions. These systems typically exhibit a liquid-like behaviour; however, in a fraction of a millisecond they can be transformed into a semi-solid-like state once exposed to an external magnetic field (**de Vicente et al., 2011**). The transformation, referred to as the MR effect, is a result of particles being aligned into chain-like structures driven by dipole-dipole interaction, thereby reinforcing the structure of the MR suspension. The particle chains are aligned along magnetic flux lines, lending an anisotropic character to these materials, macroscopically manifested as extreme change (several orders of magnitude) in viscosity, yield stress or viscoelastic moduli (**Ginder et al., 1996**). As a consequence MR suspensions play a key role in the active control of vibrations (**Li et al., 2015**), torque transducers (**Gang et al., 2019**), ultrafine polishing devices

(**Esmaeilzare et al., 2018**) and recently in the clean management of oil production (**Esmaeilnezhad et al., 2018**).

Carbonyl iron (Cl) micro-powder is currently the most popular material in magnetorheology due to its high magnetic permeability, rapid demagnetisation and widespread availability (**Felicia et al., 2013**). However, the density of this material greatly exceeds that of the carrier liquid, which causes poor sedimentation stability and complicates the redispersibility of MR suspensions, ultimately inhibiting practical applicability. Over the last few years, several approaches have been adopted to enhance the stability of MR suspensions, the most promising options comprising application of a polymer coating on the particles (**Cvek et al., 2015**) or the addition of nanoparticles (NPs) (**Hajalilou et al., 2017a**). The advantages of the former approach are concurrent enhancement of thermal oxidation stability and corrosive resistance of the particles, but subsequent MR performance is usually lower due to diminished inter-particle interactions (**Park et al., 2010**). The latter approach involving NPs enhances the magnetic permeability of the suspensions, potentially raising MR performance.

When formulating the dispersed phase of MR suspensions, it was found that binary mixtures of Cl particles enhanced packing density and MR performance (**Dodbiba et al., 2008**). Commercial Cl particles are fabricated in various grades of size. However, traditional Cl production does not provide Cl particles in a submicrometric range. This niche is often resolved by supplementation with a small addition of NPs to further increase close-packing ov the Cl (**Park et al., 2009**). Regarding the amount of NPs, it is important to note that a certain limit of them exists above which enhancement of MR response ceases. Findings have revealed that dosing ≤3% of magnetic NPs is sufficient; in fact, an excessive amount (over 7%) formed a 'halo' effect, weakening the field-induced structures (**Iglesias et al., 2012**).

The fabrication of magnetic NPs can be achieved in several ways, such as hydrothermal reactions, chemical co-precipitation, and electrochemical methods, to name just a few (**Gloag et al., 2019**). Most of these methodologies are associated with a large amount of chemical waste production, risk of contamination and toxic or hazardous chemical usage; i.e. issues detrimental to the environment (**Anastas and Eghbali, 2010**). From these reasons, there is a growing interest in the development of greener and less toxic ways to produce magnetic NPs (**Khatami et al., 2019**). For instance, iron NPs can be synthesized via environmentally-friendly methods from natural sources such as the extracts of green tea leaves or eucalyptus leaves **(Wang et al., 2014**) or other abundantly available plants (**Devath et al., 2016**). Although methods for green synthesis exist, as yet they have not been implemented to improve MR suspensions through employing the same material as the precursor for generating NPs.

In response to this challenge, the current work presents an alternative strategy to generate magnetic NPs directly from the MR suspension by applying laser fragmentation in liquids (LFL). This strategy can easily be integrated in an industrial production line to fabricate various types of NPs in almost any liquid environment. The general procedure involves the use of pulsed laser light to irradiate solid micro- or sub-microparticles, which are immersed in a liquid medium. Each solid particle absorbs the incoming laser radiation and the energy is distributed throughout the system of the particle in the form of vibrations. Depending on the amount of energy received, said laser/matter interaction promotes heating and melting, as well as consequent evaporation of the particle surface. In some cases, complete evaporation of the entire particle is achieved. This process enables the synthesis of either nanocolloids or colloidal solutions that contain a mixture of microparticles and NPs (**Pyatenko et al., 2013**). The advantages are that the LFL does not require additional hazardous chemicals to support the synthesis and the generation of by-products is minimal. Therefore, this methodology is considered an environmentally-friendly means of synthesizing NPs.

The goal of this work was to adapt LFL to facilitate a cleaner method for generating an NP-based precursor that could serve as an additive in the MR suspensions. This approach differs from any existing literature connected to magnetorheology describing the fabrication of NPs by chemical methods. Herein, NPs were generated without giving rise to any waste by-products, and their effect on the performance enhancement of the MR suspension was investigated.

2. Materials and methods

2.1. Materials

The CI particles were purchased from BASF (HQ grade, Germany), while ethylene glycol was supplied from Sigma-Aldrich (purity of ≥99%, USA). Both chemicals were used as received. The MR precursor and MR suspensions were fabricated by thorough mixing of these components in ratios described further in the text.

2.2. Laser treatment of the MR precursor

The experimental setup employed to exploit the LFL methodology for treating the MR suspension was adopted from a recent work (**Donate-Buendia et al., 2018**). Their setup had in turn been inspired by an original passage reactor proposed in 2010 for the efficient generation of colloidal nanoparticles from organic microcrystals (**Wagener and Barcikowski, 2010**). As graphically represented in **Fig. 1**, a nanosecond pulsed laser beam was focused by a cylindrical lens into a thin liquid jet that contained CI particles. The irradiated mixture was collected and redirected to feed the liquid jet again via a peristaltic pump, which ensured that the most of the CI particles interacted with the incoming laser radiation.

The laser source was an Nd:YLF unit (Litron Lasers, UK; LDY300 PIV Series, diode pumped, dual cavity). It delivers pulses at a central wavelength of 527 nm with a pulse duration of 150 ns full width at half maximum (FWHM), at a repetition rate of 1 kHz per cavity, giving out a maximum output energy of 25 mJ, and has a beam diameter of 5 mm at a width of $1/e^2$. The laser beam was focused into the liquid jet via a cylindrical lens with a focal length of 100 mm. The irradiated liquid jet was composed of a mixture of ethylene glycol and CI particles, at 30 mL and 12 mg, respectively. The concentration of the mixture was selected in accordance with recent reports dealing with similar systems (**Donate-Buendia et al., 2018**). It should be noted that ethylene glycol rarely serves as a liquid phase in magnetorheology (**Zhang et al., 2008**), but herein it represented a suitable medium for such laser treatment because it could simultaneously act as a capping agent. As a result, there is no need to add stabilising agent and stable nanocolloids are obtained (**Torres-Mendieta et al., 2019**). According to the particle heating-melting-evaporation model (**Pyatenko et al., 2013**), the laser fluence threshold required to evaporate the surface of a solid particle is $\sim$ 5 J cm^{-2}. In the current work, a laser fluence value of $\sim$ 7 J cm^{-2} was applied to ensure that sufficient energy was provided to the system to successfully carry out the evaporation process. The aforementioned laser fluence led to evaporation of the surface of the micro-particles without promoting any undesired effects, such as molecular dissociation of the ethylene glycol. The period for irradiation of the defined mixture (as above) was set to 60 min, which was selected as a compromise between the irradiated volume and gaining efficient synthesis of the NPs.

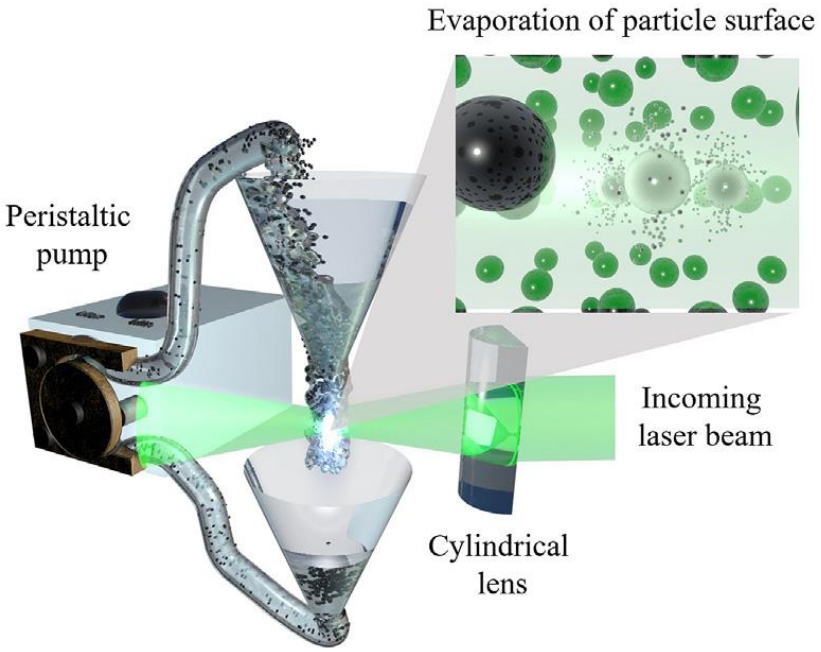

Fig. 1. Diagram of the setup for treatment of the CI particles.

2.3. Characterizations of the particles

To evaluate the differences between the original CI particles and their laser-treated analogues, various characterisation techniques were employed. The Fe content in the original sample was compared to that found in the sample after the laser treatment, which was passed through a nylon filter with a pore size of 200 nm (Agilent econofilter, 1000/pk) to determine the exact fraction of NPs created after the laser treatment. For this purpose, the corresponding solid content of both specimens was determined by inductively coupled plasma, whereby optical emission spectrometry (ICP-OES) was carried out on a spectrometer (Optima 2100DV, PerkinElmer, USA), attaining a resolution of trace elements of >0.2 ppb.

The crystallographic structure of the samples was assessed by X-ray diffraction in powder (XRD) using a diffractometer (Miniflex 600, Rigaku, Japan) with Co Kαl radiation (λ = 1.788 Å) in a 20 angle range of 10—95° at a scan speed of 1°-min^{-1}. To perform the measurements, the samples were dried through the lyophilisation process in a freeze dryer (FreeZone 2.5 L Benchtop, U.S.) at -50 °C and 0.14 mBar.

Morphology and particle dimensions were investigated by transmission electron microscopy (TEM) on an instrument (JEOL, JEM-2100Plus, Japan) equipped with a lanthanum hexaboride LaB6 cathode operating at an acceleration voltage of200 kV. The samples had been sonicated and dripped onto a carbon-coated grid (300 mesh, Agar Scientific, UK) prior to conducting the TEM analysis. Based on the images obtained, particle size distribution was analysed in consideration of ∼300 individual particles in each specimen.

The magnetic properties of the CI particles and their laser-treated analogues were investigated in a dry state on a vibrating-sample magnetometer (VSM; Model 7404, Lake Shore, USA) in magnetic fields of ±15 kOe under laboratory conditions. The samples were dosed into a VSM sample holder (730931 Kel-F, powder upper/bottom cup) mounted on a fibreglass tail with a vibration frequency of 82 Hz, vibration amplitude of 1.5 mm and time constant of 100 ms.

2.4. Magnetorheological experiments

Studying the effect of the laser-treated precursor on the performance of the MR suspension required that two MR formulations were fabricated, i.e. an additive-free MR system (reference, S1) and another modified with the NP additive (S2). In S1, the mixture of 60 wt% CI particles and 40 wt% of ethylene glycol was applied, while in S2 a fraction of 2.5 wt% of the laser-treated product was added. The homogeneity of the systems was ensured by ultrasonication (K-12LE, Kraintek, Slovakia) for 5 min.

The diluted (x 10 in ethylene glycol) MR suspensions placed on a glass substrate were exposed to an external magnetic field (200 mT) produced by permanent magnets, and the field-on particle structure formation was observed with the help of a Leica digital microscope (DVM2500, Switzerland) fitted with a VZ80C optics carrier, running LAS V4.1 software.

Finally, the MR activity of the concentrated suspensions was characterized on a rotational rheometer (MCR 502, Anton Paar, Austria), equipped with a MRD180/1T magneto-cell, PS-MRD/5A power source generating a homogeneous magnetic field in a range of up to 360 kA m^{-1} (**Cvek et al., 2016**). A sand-blasted parallel-plate (PP20/MRD/Ti/S) configuration with a gap set to 0.25 mm was employed during the experiments, while a temperature of 25 °C was maintained by a thermostatic device (Julabo FS18, Germany). To impose the same initial conditions, the MR suspensions were pre-sheared (1 min, 100 s^{-1}), and the corresponding field was applied (1 min) to the resting suspension to develop chain-like structures; this constitutes a well-established approach in MR research (**Yang et al., 2018**).

3. Results and discussion

3.1. Structural and morphological characterization

The XRD diffraction patterns displayed in **Fig. 2** detail the crystallographic structure of the CI particles and their laser-treated analogues. The CI particles exhibited peaks corresponding to cubic crystalline Fe with the symmetry space group Im-3m (COD-database: 1100108); the matching hkl planes were (110) and (200), while the lattice parameters were a = 2.861 Å, b = 2.861 Å and c = 2.861 Å. The laser-treated material displayed different peaks, among which the three most intense ones related to cubic crystalline Fe with the symmetry space group Fm-3m (COD-database: 7204807); the matching hkl planes were (111), (200) and (220), and the lattice parameters comprised a = 3.633 Å, b = 3.633 Å and c = 3.633 Å. The rest of the peaks corresponded well to cubic crystalline magnetite (Fe3O4) with the symmetry space group R-3m:H (COD-database: 1526955); the matching hkl planes were (110), (021) and (202), while the lattice parameters equalled a = 5.073 Å, b = 5.073 Å, and c = 11.427 Å.

Based on the data obtained, the largest differences between the samples pertained to expansion of the lattice of the Fe crystal and the appearance of Fe_3O_4, in line with principles of the LFL methodology. The laser radiation heated the CI particles beyond melting point (>1811 K), expanding their crystalline lattices, and changed their form from body-centred cubic to face-centred cubic arrangement (**Haynes, 2014**). Therein, high temperature led to an increment in vibrations in the crystal lattice, which in turn increased equilibrium atomic spacing, thereby causing expansion of the lattice (**Ziman, 1972**). The ethylene glycol also reacted with the evaporated material and the surfaces of the greatly heated microparticles. Different reports indicate that the laser-mediated synthesis of iron species performed in an oxygen-rich liquid medium promotes generation of various Fe oxides, most notably Fe_3O_4 (**Amendola et al., 2011**). Although LFL provides the possibility to control the size of the generated NPs, much like other similar "green" methods (**Kamali et al., 2019**), it inevitably modifies their crystallinity.

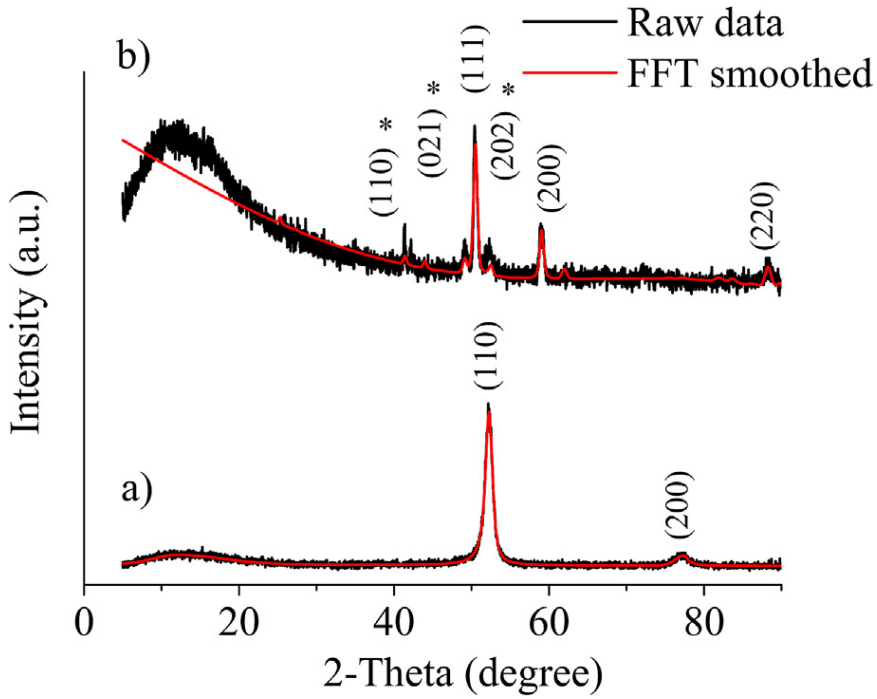

Fig. 2. XRD patterns indicating the hkl matching planes for a) the CI particles and b) the laser-treated particles (the symbol * denotes the hkl planes that match those corresponding to Fe_3O_4).

Fig. 3 shows the TEM analysis of the CI particles that had received laser radiation. As indicated above, the CI particles served as a precursor for production of the corresponding NPs. **Fig. 3**a shows that not all of the CI microparticles turned into NPs, so the resultant product could be described as a mixture of microparticles surrounded by a large amount of such NPs. The particle size distribution of the former was monomodal, with an average diameter measuring 1122.3 ± 665.4 nm (**Fig. 3**b). This value is similar to that provided by the manufacturer (d_{50} value of 2 µm via the laser-diffraction method). In contrast the NPs exhibited a bimodal size distribution (**Fig. 3**c and d), their average diameters equalling 2.6 ± 1.8 nm and 17.8 ± 9.1 nm, respectively. In more details, the NPs produced were almost spherical in shape, and their coexistence with the microparticles is a highly advantageous situation as it increases close-packing of the particles (**Iglesias et al., 2012**). The TEM images reveal that the NPs show a great potential for being incorporated in field-induced particle chains. Indeed, ICP-OES measurements indicated that the real content of the NPs was approximately 24.9 wt% in the laser-treated fraction. Therefore, in S2 it was specifically added 0.62 wt% of the NPs and 1.8 wt% of laser-irradiated microparticles. Various papers state that even though the limit of ≤3% NPs is suitable for enhancing MR suspensions, it is more typical to use 0.5—1.5 wt% to avoid an undesirable increase in off-state viscosity/shear stress in real-world applications (**Esmaeilnezhad et al., 2017; Li et al., 2015**).

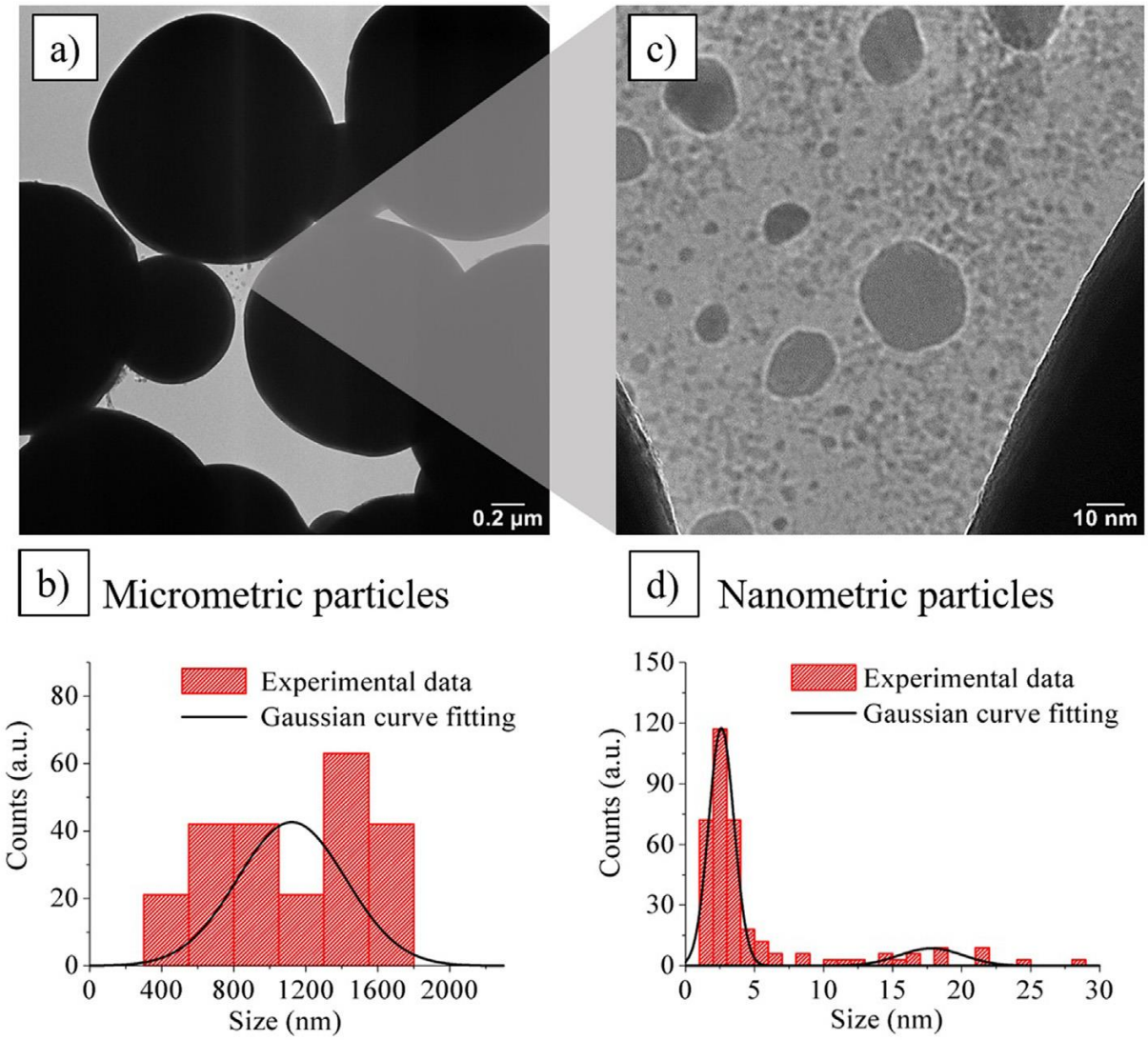

Fig. 3. Representative TEM micrographs of the MR suspension after laser irradiation; a) a general view of the sample, b) a histogram corresponding to the size of the micrometric particles, c) a magnified view of the particles and d) a histogram corresponding to the size of the NPs.

3.2. Magnetic properties

The isothermal magnetic behaviour of the CI particles and their laser-treated analogues is illustrated in **Fig. 4**. The former exhibited an S-shaped characteristic, suggesting ferromagnetic behaviour, with negligible coercivity, indicative of the potential for rapid demagnetisation. According to the model proposed by Jiles—Atherton (J—A) (Liorzou et al., 2000), the saturation magnetisation, MS, of the CI particles reached values of over 200 emu-g^{-1}, as similarly reported elsewhere (**Kim et al., 2016**). On the other hand, the NP analogues (**Fig. 2**b) were characterized by a coercivity of 8.4 kA m^{-1}, a remnant magnetisation of 1.8 emu . g^{-1} and a mean value for MS estimated as 42.7 emu . g^{-1}. Note that the laser-treated NP fraction might have contained a portion of non-irradiated particles, therefore its M_S value was designated as "mean".

The value for M_S gauged for the NPs, which was lower than for the CI particles, was expected due to the average particle size. The given magnetic properties originate from two primary mechanisms — spin rotation and domain wall movement. Since the latter is dominant in ferromagnetism and requires less energy, it is logical that the multi-domain CI particles demonstrated a higher MS value. A

consequence of their greater size, this increased the possibility of attaining domain wall movement (Hajalilou et al., 2017b). Otherwise the coercivity of both materials was in accordance with the well-accepted law α 1 /D, where D represents mean particle diameter (**Hajalilou et al., 2015**). This proved that the CI particles were ideal for the composition of the MR suspension, in which a rapid field-induced switch-like behaviour was required. The slightly higher coercivity of the NPs supported the hypothesis that excessive doses of them in the MR suspension could lengthen response time and cause steric problems during the particle structure formation.

Regarding the fitting procedure, it should be noted that the J—A model exhibited excellent close-fitting capabilities for the magnetisation data of the NPs. In the case of the CI particles, the mathematical prediction was still reasonable but a mismatch with the data appeared in the transition from the unsaturated state to a deeply saturated state (**Fig. 5**).

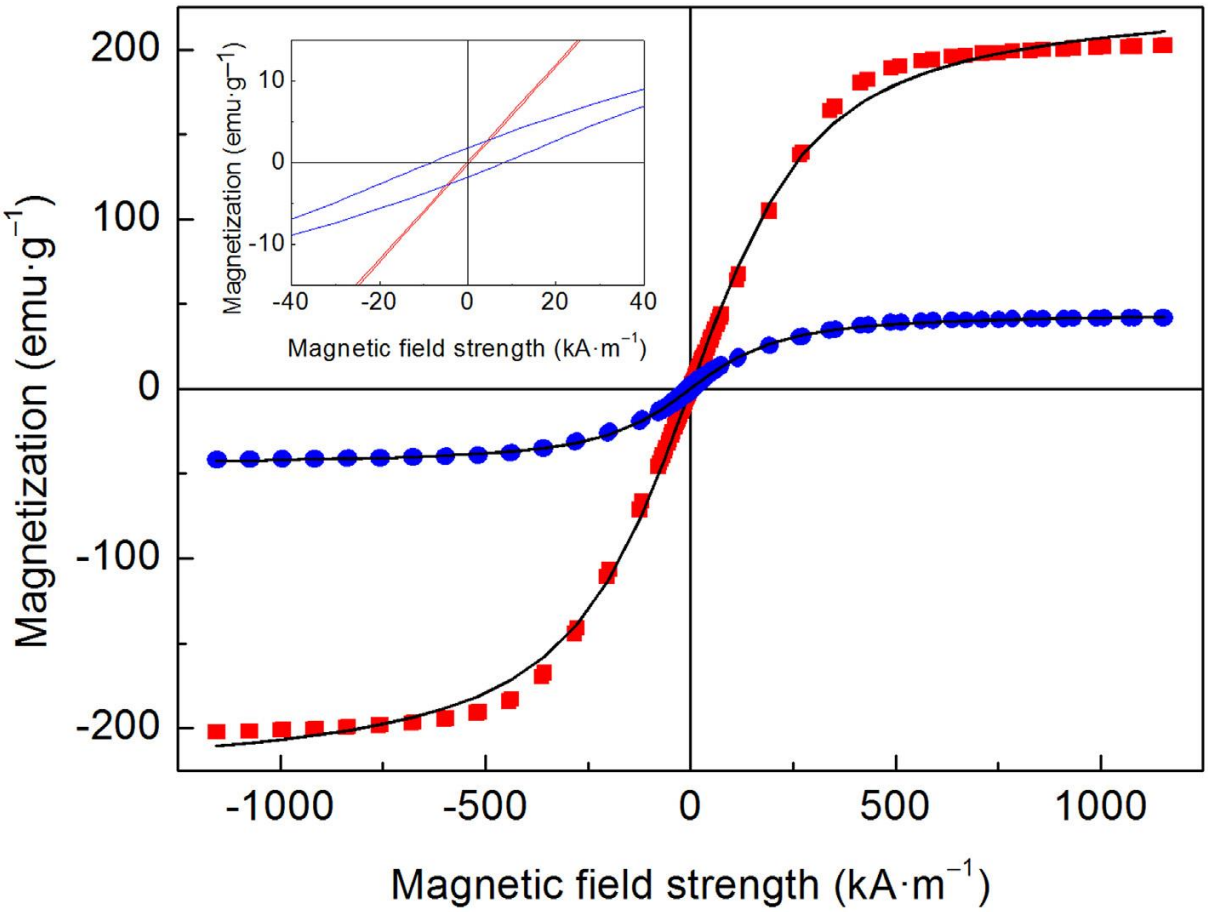

Fig. 4. VSM hysteresis loops for the CI particles (squares) and their laser-treated NP analogues (circles). The inset displays magnification of the zero-field region.

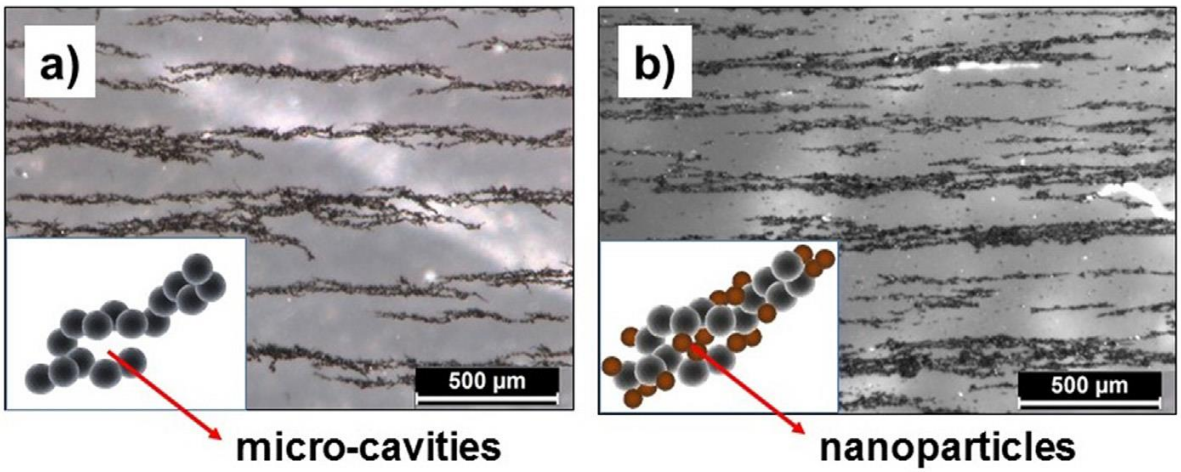

Fig. 5. Detailed views of field-induced particle structures in: a) the diluted MR suspension, and b) its analogue containing the laser-produced NPs.

This can be explained by the inherent nature of the J—A model, since parameters related to rotation domain are not introduced in the model (**Zhang et al., 2018**). Overall, the laser-treated fraction exhibited reasonable magnetisation values, indicating that their active incorporation had occurred in the CI structures; thus an enhanced MR response could be anticipated.

3.3. Field-induced structuration and MR aktivity

Detailed optical images of field-induced particle structures are considered a suitable means for predicting their stiffness and showing the impact of various additives (**Hajalilou et al., 2017a**, **2017b**) across the magneto- and electro-rheology (**Mrlik et al., 2018**). Such visualisations are given in **Fig. 5**, and reveal that the reference MR suspension, S1, exhibited lower particle-chain uniformity than its analogue, S2, with the laser-treated particles. In the latter suspension, the fraction of the laser-produced NPs provided enhanced connectivity between the CI particles, this constituting the main premise for enhancing permeability and particle-chain rigidity.

Evaluating any enhancements due to the NPs co-existence in the MR suspensions involved measuring rheological characteristics under conditions of exposing the S1 and S2 specimens to an external magnetic field. The subsequent data were fitted via the Robertson—Stiff (R—S) viscoplastic model. As visible in **Fig. 6**, shear stress and shear rate followed a non-linear trend across the entire range of magnetic field strengths. Thus, the most popular viscoplastic model, i.e. the Bingham plastic model (Iglesias et al., 2012), could not be accurately applied. Out of the various non-linear models in existence, the R—S model was selected as it appeared to possess superior fitting/predictive capabilities for the given types of flow curves (**Cvek et al., 2016**). The close-fitting effectiveness of the R—S model was evidenced by reliable description of the data and a high correlation coefficient (R^2 > 0.97) in most cases.

Fig. 6 reveals that both of the MR suspensions exhibited nearly Newtonian behaviour in the absence of a magnetic field. Specifically, S2 displayed certain non-Newtonian traits, most likely due to increased particle friction and remnant magnetisation of the NPs (**Fig. 4**, inset).

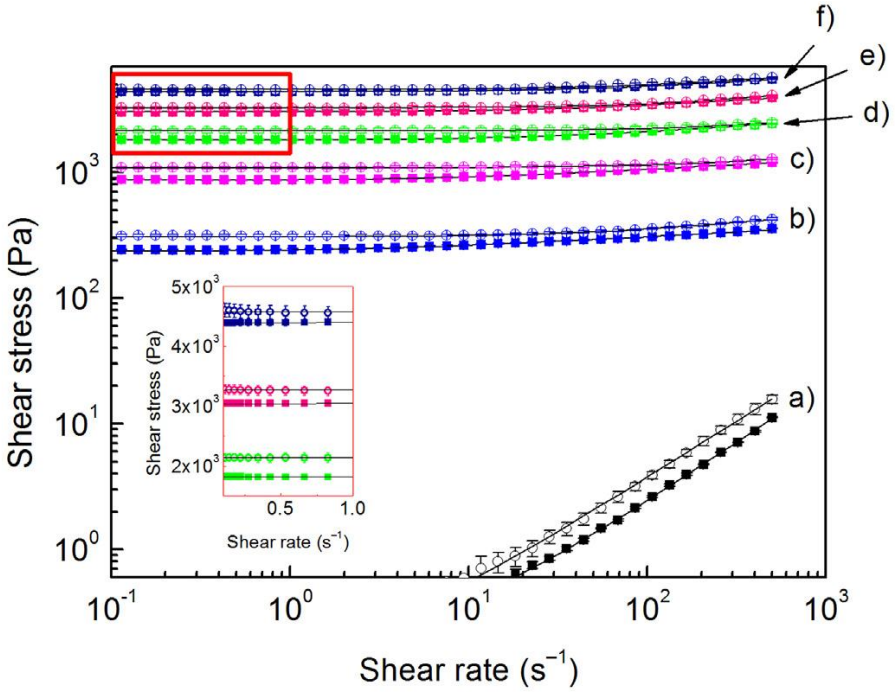

Fig. 6. Representative rheological data for S1 (squares) and S2 (circles) under the magnetic field strengths of 0, 72,144,216,288 and 360 kA m^{-1} (a—f). The inset shows a magnified view of the selected region as lin—lin coordinates to emphasise difference in shear stress values. The solid lines refer to the best predictions of the R—S model.

This result was supported by the value reported for the fitting n-index, which dropped from 0.96 to 0.90 (for Newtonian fluids n-index equals 1). After imposing the field, a significant increase in shear stress values accompanied with the appearance of yield stress was observed, which is a typical feature for moderately to highly concentrated MR suspensions (**de Vicente et al., 2011**).

In absolute values, S2 exhibited notably enhanced shear stress values attributable to the presence of the NPs (**Fig. 3**). The mechanism of such enhancement can be explained as follows: despite the fact that a certain limitation in the close-packing of microparticles exists, NPs are easily accommodated among Cl particles, where they serve as pathways for magnetic flux lines (**Yang et al., 2018**), with the subsequent effect of mechanically anchoring the internal structures (**Hajalilou et al., 2017a**). In contrast to electrorheological fluids (**Esmaeilnezhad and Choi, 2019**), the stiffening effect was significantly higher, further evidencing the practical applicability of the developed system.

As is widely known, the most relevant quantity of MR suspensions is yield stress, which is associated with their efficiency (**Bossis et al., 2002**). Herein, dynamic yield stress, ty, according to predictions based on the R—S model, was further used to evaluate the performance of the tested suspensions. As reported earlier (**Ginder et al., 1996**), ty is a non-trivial function of the magnetic field applied, due to magnetic non-linearity and the existence of saturation magnetisation. In this function, two primary regions/slopes can be distinguished. Under low fields, ty primarily depends on magnetic field intensity and it scales as f H^2. However, beyond a certain threshold, which is referred to as the "critical field", HC, ty increases in accordance with f $H^{3/2}$ since MS then becomes more relevant.

As visualized in **Fig. 7**, the rise in ty was in line with the theoretical model, with only small deviations being observed. These potentially stemmed from the use of the R—S model as the yield stress predictor as well as the moderate particle weight fraction in the tested suspensions. Note that the literature describes MR suspensions of medium concentration as only exhibiting one regime with a slope of 1.5 throughout a wide range of magnetic field strengths (**Esmaeilnezhad et al., 2017**), and the

finding herein of single-regime behaviour is in good agreement with this. Unlike the S1 suspension, S2 exhibited enhanced ty values and a slightly higher slope of dependence, which suggests that the NPs facilitated magnetisation of the CI particles, although the HC value remained similar.

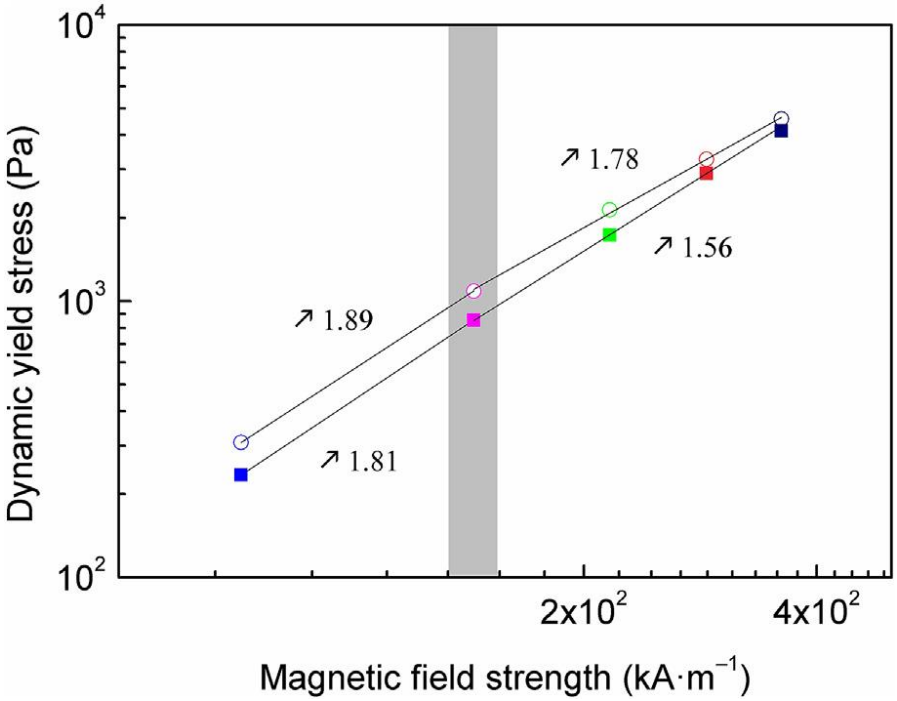

Fig. 7. Dynamic yield stress plotted against magnetic field strength for S1 (squares) and S2 (circles). The solid lines refer to theoretical slopes as per the method devised by Ginder. The grey band denotes the HC region.

It was also evident (**Fig. 7**) that the importance of the NPs was significant in magnetic fields of low to moderate strength, demonstrating up to 31% in enhancement, while in higher fields such difference become less obvious (only 6.4%). The latter situation can be explained as a consequence of reaching values for MS at which it is preferable to release the gap between two particles. A similar conclusion was recently drawn by other researchers (**Yang et al., 2018**), who experimented with ternary MR suspensions (solid-ferrofluid-liquid systems), which might constitute an analogy for the research conducted in this paper. The enhancements in ty (in dozens of per cent) achieved by utilizing laser-generated NPs could be considered comparable with results of ones fabricated via conventional chemical methods (**Leong et al., 2016**).

To conclude, the NP-based additive produced using the LFL methodology served as an efficient, close-packing and enhancing element in the MR suspensions, where it heightened the most relevant MR property represented by ty. This implies that various MR devices can readily benefit from this clean and effective technology, including, but not limited to, vibration absorbers, brakes, thermal energy transfer devices and control valves (**de Vicente et al., 2011**). As MR performance was predominantly enhanced in the region of a low to moderate magnetic field region, a great potential is expected mainly in for small robotic systems operating in such a magnetic field region, e.g. a pen-like haptic interface (**Chen et al., 2018**) or MR-based systems for teleoperations (**Gang et al., 2019**).

4. Conclusions

Due to increase in the level of interest shown for magnetic NPs in the development of efficient smart fluids, it has become essential to explore alternative means of production that minimize any environmental impact. Herein, the authors present a facile, environmentally-friendly and waste-free producing perspective for improving MR suspensions via a nanoscale additive approach. The NP-based additive was produced directly from the given MR suspension through applying the LFL technique. This permitted controlled generation of almost spherical crystalline Fe_3O_4 and cubic crystalline Fe NPs, primarily of 2.6 ± 1.8 nm and 17.8 ± 9.1 nm in dimension, which demonstrated a reasonable MS value of approximately 42.7 emu g^{-1}. The effect of the NPs on the performance of the MR suspension was evaluated by analysing their structural and rheological characteristics. Incorporating the laser-treated additive into the MR suspension enhanced the connectivity of the CI microparticles and facilitated their magnetisation, resulting in notably enhanced field-induced shear stress values. Improvement in MR performance occurred predominantly in the region of a low to moderate magnetic field, equating to 31% in enhancement of ty, highlighting the efficiency of the laser-synthesized additive. Consequently, the laser-based method was demonstrated to be an environmentally-friendly means for designing bidispersed MR suspensions with enhanced performance. The approach described is a clean alternative to standard chemical procedures for fabricating magnetic NPs and brings about equivalent levels of enhancement. The future challenges can be perceived in further optimizing the laser treatment process and scaling up the production for industrial purposes, with potential applications including field-driven robotics and torque or damping systems.

References

Amendola, V., Riello, P., Meneghetti, M., 2011. Magnetic nanoparticles of iron carbide, iron oxide, iron@iron oxide, and metal iron synthesized by laser ablation in organic solvents. J. Phys. Chem. C 115, 5140—5146. https://doi.org/10.1021/ jp109371m.

Anastas, P., Eghbali, N., 2010. Green chemistry: principles and practice. Chem. Soc. Rev. 39, 301—312. https://doi.org/10.1039/b918763b.

Bossis, G., Lacis, S., Meunier, A., Volkova, O., 2002. Magnetorheological fluids. J. Magn. Magn Mater. 252, 224—228. https://doi.org/10.1016/s0304-8853(02) 00680- .

Chen, D.P., Song, A.G., Tian, L., Yu, Y.Q., Zhu, L.F., 2018. MH-Pen: a pen-type multimode haptic interface for touch screens interaction. IEEE Trans. Haptics 11, 555—567. https://doi.org/10.1109/toh.2018.2826551.

Cvek, M., Mrlik, M., Ilcikova, M., Plachy, T., Sedlacik, M., Mosnacek, J., Pavlinek, V., 2015. A facile controllable coating of carbonyl iron particles with poly(glycidyl methacrylate): a tool for adjusting MR response and stability properties. J. Mater. Chem. C 3, 4646—4656. https://doi.org/10.1039/c5tc00319a.

Cvek, M., Mrlik, M., Pavlinek, V., 2016. A rheological evaluation of steady shear magnetorheological flow behavior using three-parameter viscoplastic models. J. Rheol. 60, 687—694. https://doi.org/10.1122/1.4954249.

de Vicente, J., Klingenberg, D.J., Hidalgo-Alvarez, R., 2011. Magnetorheological fluids: a review. Soft Matter 7, 3701—3710. https://doi.org/10.1039/c0sm01221a.

Devath, C.P., Thalla, A.K., Katte, S.Y., 2016. Green synthesis of iron nanoparticles using different leaf extracts for treatment of domestic waste water. J. Clean. Prod. 139, 1425—1435. https://doi.org/10.1016/j.jclepro.2016.09.019.

Dodbiba, G., Park, H.S., Okaya, K., Fujita, T., 2008. Investigating magnetorheological properties of a mixture of two types of carbonyl iron powders suspended in an ionic liquid. J. Magn. Magn Mater. 320, 1322—1327. https://doi.org/10.1016/ j.jmmm.2007.10.03 .

Donate-Buendia, C., Torres-Mendieta, R., Pyatenko, A., Falomir, E., Fernandez-Alonso, M., Minguez-Vega, G., 2018. Fabrication by laser irradiation in a continuous flow jet of carbon quantum dots for fluorescence imaging. ACS Omega 3, 2735—2742. https://doi.org/10.1021/acsomega.7b02082.

Esmaeilnezhad, E., Choi, H.J., 2019. Polyindole nanoparticle-based electrorheological fluid and its green and clean future potential conformance control technique to oil fields. J. Clean. Prod. 231, 1218—1225. https://doi.org/10.1016/ j.jclepro.2019.05.341.

Esmaeilnezhad, E., Choi, H.J., Schaffie, M., Gholizadeh, M., Ranjbar, M., Kwon, S.H., 2017. Rheological analysis of magnetite added carbonyl iron based magnetorheological fluid. J. Magn. Magn Mater. 444, 161—167. https://doi.org/10.1016/ j.jmmm.2017.08.023.

Esmaeilnezhad, E., Choi, H.J., Schaffie, M., Gholizadeh, M., Ranjbar, M., 2018. Polymer coated magnetite-based magnetorheological fluid and its potential clean procedure applications to oil production. J. Clean. Prod. 171, 45—56. https:// doi.org/10.1016/j.jclepro.2017.10.004.

Esmaeilzare, A., Rezaei, S.M., Ramezanzadeh, B., 2018. Corrosion and magnetic properties of encapsulated carbonyl iron particles in aqueous suspension by inorganic thin films for magnetorheological finishing application. Appl. Surf. Sci. 436, 1200—1212. https://doi.org/10.1016/j.apsusc.2017.12.135.

Felicia, L.J., Reji, J., Philip, J., 2013. Rheological properties of magnetorheological fluid with silica nanoparticles stabilizers — a comparison with ferrofluid. J. Nanofluids 2, 75—84. https://doi.org/10.1166/jon.2013.1047.

Gang, H.G., Choi, S.B., Sohn, J.W., 2019. Experimental performance evaluation of a MR brake-based haptic system for teleoperation. Front. Mater. 6, 25. https:// doi.org/10.3389/fmats.2019.00025.

Ginder, J.M., Davis, L.C., Elie, L.D., 1996. Rheology of magnetorheological fluids: models and measurements. Int. J. Mod. Phys. B 10, 3293—3303. https://doi.org/ 10.1142/s0217979296001744.

Gloag, L., Mehdipour, M., Chen, D.F., Tilley, R.D., Gooding, J.J., 2019. Advances in the application of magnetic nanoparticles for sensing. Adv. Mater. 1904385. https:// doi.org/10.1002/adma.201904385.

Hajalilou, A., Hashim, M., Kamari, H.M., Masoudi, M.T., 2015. Effects of milling atmosphere and increasing sintering temperature on the magnetic properties of nanocrystalline Ni0.36Zn0.64Fe2O4. J. Nanomater. 615739. https://doi.org/ 10.1155/2015/615739.

Hajalilou, A., Kianvash, A., Shameli, K., Lavvafi, H., 2017a. Carbonyl iron based magnetorheological effects with silver nanoparticles via green-assisted coating. Appl. Phys. Lett. 110, 261902. https://doi.org/10.1063/h4990679.

Hajalilou, A., Mazlan, S.A., Shilan, S.T., Abouzari-Lotf, E., 2017b. Enhanced magnetorheology of soft magnetic carbonyl iron suspension with binary mixture of Ni-Zn ferrite and Fe3O4 nanoparticle additive. Colloid Polym. Sci. 295, 1499—1510. https://doi.org/10.1007/s00396-017-4128-3.

Haynes, W.M., 2014. Handbook of Chemistry and Physics. CRC Press, Boca Raton, FL.

Iglesias, G.R., Lopez-Lopez, M.T., Duran, J.D.G., Gonzalez-Caballero, F., Delgado, A.V., 2012. Dynamic characterization of extremely bidisperse magnetorheological fluids. J. Colloid Interface Sci. 377, 153—159. https://doi.org/10.1016/ j.jcis.2012.03.07 .

Kamali, M., Costa, M.E.V., Otero-Irurueta, G., Capela, I., 2019. Ultrasonic irradiation as a green production route for coupling crystallinity and high specific surface area in iron nanomaterials. J. Clean. Prod. 211, 185—197. https://doi.org/10.1016/ jjclepro.2018.n.12 .

Khatami, M., Alijani, H.Q., Fakheri, B., Mobasseri, M.M., Heydarpour, M., Farahani, Z.K., Khan, A.U., 2019. Super-paramagnetic iron oxide nanoparticles (SPIONs): greener synthesis using Stevia plant and evaluation of its antioxidant properties. J. Clean. Prod. 208, 1171—1177.https://doi.org/10.1016/ j.jclepro.2018.10.182.

Kim, M.W., Han, W.J., Kim, Y.H., Choi, H.J., 2016. Effect of a hard magnetic particle additive on rheological characteristics of microspherical carbonyl iron-based magnetorheological fluid. Colloids Surf., A 506, 812—820. https://doi.org/ 10.1016/j.colsurfa.2016.07.070.

Leong, S.A.N., Samin, P.M., Idris, A., Mazlan, S.A., Rahman, A.H.A., 2016. Synthesis, characterization and magnetorheological properties of carbonyl iron suspension with superparamagnetic nanoparticles as an additive. Smart Mater. Struct. 25, 025025 https://doi.org/10.1088/0964-1726/25/2/025025.

Li, J.H., Wang, W., Xia, Y., He, H., Zhu, W.H., 2015. The soft-landing features of a micro-magnetorheological fluid damper. Appl. Phys. Lett. 106, 014104 https:// doi.org/10.1063/1.4903924.

Liorzou, F., Phelps, B., Atherton, D.L., 2000. Macroscopic models of magnetization. IEEE Trans. Magn. 36, 418-428. https://doi.org/10.1109/20.825802.

Mrlik, M., Ilcikova, M., Plachy, T., Moucka, R., Pavlinek, V., Mosnacek, J., 2018. Tunable electrorheological performance of silicone oil suspensions based on controllably reduced graphene oxide by surface initiated atom transfer radical polymerization of poly(glycidyl methacrylate). J. Ind. Eng. Chem. 57, 104-112. https://doi.org/10.1016/jjiec.2017.08.013.

Park, B.J., Song, K.H., Choi, H.J., 2009. Magnetic carbonyl iron nanoparticle based magnetorheological suspension and its characteristics. Mater. Lett. 63, 1350-1352. https://doi.org/10.1016/j.matlet.2009.03.013.

Park, B.J., Fang, F.F., Choi, H.J., 2010. Magnetorheology: materials and application. Soft Matter 6, 5246-5253. https://doi.org/10.1039/c0sm00014k.

Pyatenko, A., Wang, H.Q., Koshizaki, N., Tsuji, T., 2013. Mechanism of pulse laser interaction with colloidal nanoparticles. Laser Photon. Rev. 7, 596-604. https:// doi.org/10.1002/lpor.201300013.

Torres-Mendieta, R., Havelka, O., Urbanek, M., Cvek, M., Waclawek, S., Padil, V.V.T., Jasikova, D., Kotek, M., Cernik, M., 2019. Laser-assisted synthesis of Fe-Cu oxide nanocrystals. Appl. Surf. Sci. 469, 1007-1015. https://doi.org/10.1016/ j.apsusc.2018.11.058.

Wagener, P., Barcikowski, S., 2010. Laser fragmentation of organic microparticles into colloidal nanoparticles in a free liquid jet. Appl. Phys. Mater. Sci. Process 101, 435-439. https://doi.org/10.1007/s00339-010-5814-x.

Wang, T., Lin, J.J., Chen, Z.L., Megharaj, M., Naidu, R., 2014. Green synthesized iron nanoparticles by green tea and eucalyptus leaves extracts used for removal of nitrate in aqueous solution. J. Clean. Prod. 83, 413-419. https://doi.org/10.1016/ j.jclepro.2014.07.006.

Yang, J.J., Vereda, F., Morillas, J.R., de Vicente, J., 2018. Ternary solid-ferrofluid-liquid magnetorheological fluids. Smart Mater. Struct. 27, 075017 https://doi.org/ 10.1088/1361-665X/aac4c9.

Zhang, X.Z., Li, W.H., Gong, X.L., 2008. Study on magnetorheological shear thickening fluid. Smart Mater. Struct. 17, 015051 https://doi.org/10.1088/0964-1726/ 17/1/015051.

Zhang, H., Liu, Y., Liu, S.W., Lin, F.C., 2018. Application of Jiles-Atherton model in description of temperature characteristics of magnetic core. Rev. Sci. Instrum. 89, 104702. https://doi.org/10.1063/1.5050687.

Ziman, J.M., 1972. Principles of the Theory of Solids. Cambridge University Press, Cambridge.